coatings

MDPI

Article

Effect of HfO_2 Particles on Ceramic Coating Fabricated on Ti6Al4V Alloy via Plasma Electrolytic Oxidation

Manxi Sun [1], Meiling Jiang [2], Hongjian Huang [2,*], Biao Yang [3], Yuhang Lin [3] and Ping Wang [3]

[1] School of Mechanical and Engineering, Xihua University, Chengdu 610039, China
[2] College of Materials Science and Engineering, Xihua University, Chengdu 610039, China
[3] School of New Energy and Materials, Southwest Petroleum University, Chengdu 610500, China; 818wp@163.com (P.W.)
* Correspondence: hongjianhuang1021@yeah.net

Abstract: Hafnium dioxide (HfO_2) has a wide bandgap and high dielectric constant. We prepared ceramic coatings on Ti6Al4V alloys via plasma electrolytic oxidation (PEO) in an electrolyte with HfO_2 particles. The influence of the HfO_2 particles on the microstructure, phase composition, elemental distribution, and corrosion resistance of the PEO coatings was systematically investigated. The results showed that the addition of HfO_2 increased the oxidation voltage (from 462 to 472 V) and promoted the microarc sintering reaction so that the thickness and hardness of the resulting PEO coating increased. Moreover, the quantity of the micropores on the coating surface caused by the discharge decreased after adding the HfO_2 particles. The X-ray diffraction patterns confirmed that the HfO_2 particles were incorporated into the coating by remelting and sintering the microarc. Furthermore, the corrosion resistance of the PEO coating was remarkably increased after introducing HfO_2, which was attributed to the increase in the electrode potential and the densification of the coating structure.

Keywords: plasma electrolytic oxidation; Ti6Al4V; hafnium oxide particles; corrosion resistance

Citation: Sun, M.; Jiang, M.; Huang, H.; Yang, B.; Lin, Y.; Wang, P. Effect of HfO_2 Particles on Ceramic Coating Fabricated on Ti6Al4V Alloy via Plasma Electrolytic Oxidation. *Coatings* **2023**, *13*, 967. https://doi.org/10.3390/coatings13050967

Received: 7 April 2023
Revised: 18 May 2023
Accepted: 19 May 2023
Published: 22 May 2023

1. Introduction

The Ti6Al4V titanium alloy is regarded as an important structural material in the petrochemical, aerospace, and deep-sea-ships industries due to its high corrosion resistance, toughness, and weldability [1–4]. However, with the development of the petrochemical industry, the Ti6Al4V titanium alloy cannot function in some harsh environments. Therefore, using appropriate technology to increase the wear, thermal shock, and corrosion resistance of the Ti6Al4V titanium alloy is necessary [5,6].

Plasma electrolytic oxidation (PEO), also called microarc oxidation (MAO), has been one of the commonly used surface treatment technologies for valve metals (aluminum, magnesium, titanium, and zirconium as well as their alloys) in recent years [7–9]. The ceramic coatings, which have the advantages of wear and corrosion resistance, low thermal conductivity, and a high bonding strength with the substrate, can be fabricated via PEO [10–12]. In general, the PEO coatings are formed both by substrate oxidation and by other electrolyte substances deposited onto the substrate surface, which allows for a wide range of modifications of the coating's composition and properties. For specific purposes, fine powders of hard, high-melting-point materials and/or dry lubricants (for enhanced friction and wear) and/or coloring agents (for optical properties and decoration) can be introduced into the electrolytes to integrate the cataphoretic effects into the oxidation process. Many researchers have focused on modifying PEO coatings based on the above theory.

Yang et al. [13] found that AlN-doped PEO coatings had an excellent thermal conductivity and insulation performance due to the AlN properties. Li et al. [11] found that the addition of ZrO_2 particles could increase the oxidation and wear resistance of PEO coatings. Chen et al. [14] fabricated graphene and PEO coatings and found an increase in the hardness and corrosion resistance compared with a single PEO coating. Zheng et al. [15]

reported that PEO coatings with CeO_2 particles exhibited excellent corrosion resistance with a self-sealing ability. Ma et al. [16] revealed that the addition of B_4C/C particles during the PEO process resulted in an increase in the thickness and a decrease in the friction coefficient of the as-prepared PEO coating. Liu et al. [17] found that the addition of BiS_2 increased the thickness and hardness of the PEO coating, but its thermal shock resistance decreased. In general, researchers are still actively exploring the use of particle or component additives to enhance the properties of PEO coatings.

Hafnium oxide (HfO_2) is attracting attention in the ceramic industry due to its wide bandgap, high dielectric constant, excellent corrosion resistance, and thermal and chemical stability [18–20], and the high impedance of HfO_2 films was confirmed by Esplandiu et al. [21]. Therefore, HfO_2 is expected to enhance the properties of PEO coatings fabricated on Ti6Al4V, especially their corrosion resistance.

Herein, HfO_2 particles as an additive during the PEO process are first reported, and the influence of HfO_2 particles on PEO coatings was systematically investigated. The components and compositions of the PEO coating indicated that the HfO_2 was successfully introduced into the coating through remelting caused by the plasma discharge instead of a new compound. With the introduction of HfO_2, the insulation property of the PEO coating was increased, which led to an increase in the oxidation voltage and more severe plasma breakdown. Thus, more electrolyte components could be sintered onto the PEO coating, which resulted in an increase in the coating thickness. Moreover, the hardness and corrosion resistance of the HfO_2-doped coating were higher than those of the nondoped coating due to the densification of the coating.

2. Experimental Procedure

2.1. Sample Preparation

The Ti6Al4V samples had dimensions of $15 \times 15 \times 3$ mm^3. The main elements of the contents (mass percentage) were (5.5~6.8%) Al, (3.5~4.5%) V, (0.3%) Fe, (0.15%) Si, (0.1%) C, (0.05%) N, and (0.2%) O, with Ti balance. Prior to the PEO coating preparation, the Ti6Al4V samples were ground with abrasive papers (400-2000#) and then cleaned with deionized water for use.

The PEO processes were conducted at a peak current density of 10 A/dm^2 for 30 min with a fixed frequency of 500 Hz and a duty cycle of 50%. The selected electrolyte formulations were Na_2SiO_3 (4 g/L), Na_3PO_4 (6 g/L), NaOH (0.5 g/L), EDTA (0.3 g/L), and $C_3H_8O_3$ (3 mL/L). In addition, HfO_2 was added to the electrolyte as an additive (5 g/L). Both the basic and modified electrolyte were stirred and placed for 24 h before the PEO process to make the ions in the solution more stable. During the PEO process, the electrolyte temperature was maintained at 25 ± 5 °C, and it was continuously and mechanically stirred. Finally, the samples were sealed with 95 ± 5 °C deionized water for 20 min, and then they were naturally cooled in the air.

2.2. Coating Characterization

The morphology of the coatings was investigated by using scanning electron microscopy (SEM, ZEISS EVO MA15, Oberkochen, Germany), and the elemental content and distribution were detected via energy dispersive spectroscopy (EDS, OXFORD 20, Carl Zeiss Microscopy GmbH, Oberkochen, Germany) coupled to the SEM. The compositions of the coatings were determined by using X-ray diffraction (XRD, DX-2700B, Liaoning, China) with a scanning speed of 0.04°/s and a range of 2θ from 10° to 80°. An X-ray photoelectron spectrometer (XPS, ESCALAB 250X, Waltham, MA, USA) was used to detect the target elements. A digital microhardness tester (HXD-2000TM/LCD, Chengdu, China) was used to evaluate the surface hardness of the coating at a load of 1 N for 15 s, five points were measured for each sample, and the average value was recorded. The thickness and roughness of the coatings were measured by using an eddy current thickness gauge (TT230, Beijing, China) and a surface roughness meter (HD350, Beijing, China), respectively. A Tafel plot and electrochemical impedance spectroscopy (EIS) of the PEO coatings were evaluated

by using an electrochemical workstation (Reference 3000, Philadelphia, Commonwealth of Pennsylvania, Harrisburg, PA, USA) with a saturated calomel electrode (SCE) as the reference in a 3.5 wt.% NaCl solution.

3. Results and Discussion

3.1. Voltage–Time Response

Figure 1 shows the voltage–time response curves before and after HfO_2 was added during the PEO process. Three stages were clearly observed on the two curves. From 0 to 1 min, a passivation film with a high impedance was rapidly formed on the surface of the Ti6Al4V anode after the circuit was turned on, which resulted in a sharp rise in the voltage, which indicated the general anodization stage [22]. In this stage, the slopes of the two voltage–time curves were roughly the same. Subsequently, when the oxidation voltages increased to the breakdown voltages (355 and 367 V for the PEO and PEO + HfO_2 samples, respectively), we observed that a soft spark with low brightness appeared on the anode surface (called the sparking anodization stage). The discontinuous PEO ceramic coating began to form on the surface of the sample, and the weak parts of the coating were constantly broken down by soft sparks [23]. As shown in Figure 1, the PEO + HfO_2 sample showed a relatively higher voltage rise rate than the PEO sample in the 1 to 3 min stage. Finally, the two voltage–time response curves reached the plateau voltages (~462 and ~476 V for the PEO and PEO + HfO_2 samples, respectively) for the 3 to 30 min stage and then slowly increased. In this stage, we observed that the number of sparks decreased and the intensity considerably increased (also called microarcs), which indicated a higher sintering temperature and pressure around the spark-modification area. The higher plateau voltages of the PEO + HfO_2 sample suggest that adding HfO_2 can change the discharge characteristics during the PEO process, which facilitates the deposition of HfO_2 particles on the coating.

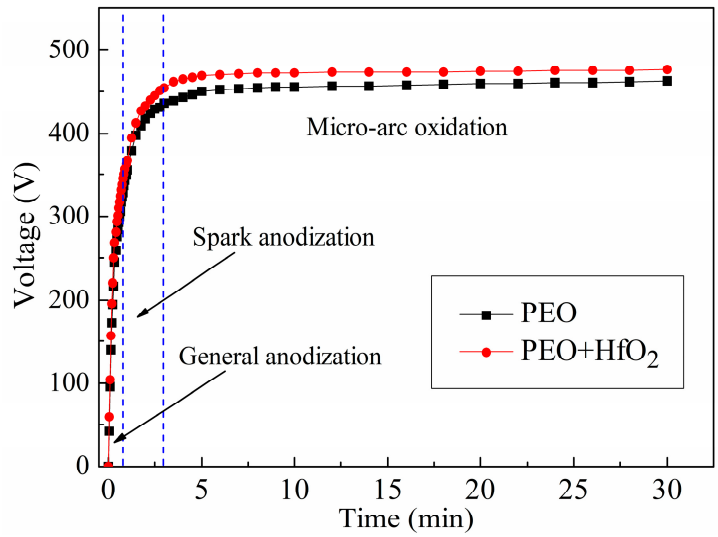

Figure 1. Voltage–time response curves of PEO and PEO + HfO_2 coating.

3.2. Morphology of the Coatings

The SEM morphology and the element distribution on the surface of the PEO and PEO + HfO_2 samples are presented in Figure 2. Many micropores were present on the surface of the two samples, which were generated by the release of a gas associated with the PEO process, and the micropores were surrounded by volcanic-rock-like stacks [24]. Regarding the surface of the sample without HfO_2 (Figure 2a), many small-sized micropores could be observed; by contrast, the quantity of the discharge micropores of the coating decreased and the size increased after the HfO_2 particles were added (Figure 2b). With the increase in the oxidation voltage (after adding HfO_2), the amount of melt ejected

through the discharge micropores increased, and part of the melt solidified around the micropores due to the liquid quenching by the electrolyte. Due to the repeated melting and solidification of the volcanic-rock-like stacks, the various micropores were welded together so that the size of the micropores increased, and thus some small micropores were closed and disappeared. Moreover, the rougher surface of the PEO + HfO_2 coating (Ra = 1.268 μm) compared with the PEO coating (Ra = 0.847 μm) could also be attributed to the more violent discharge process under the high voltage (Figure 2b).

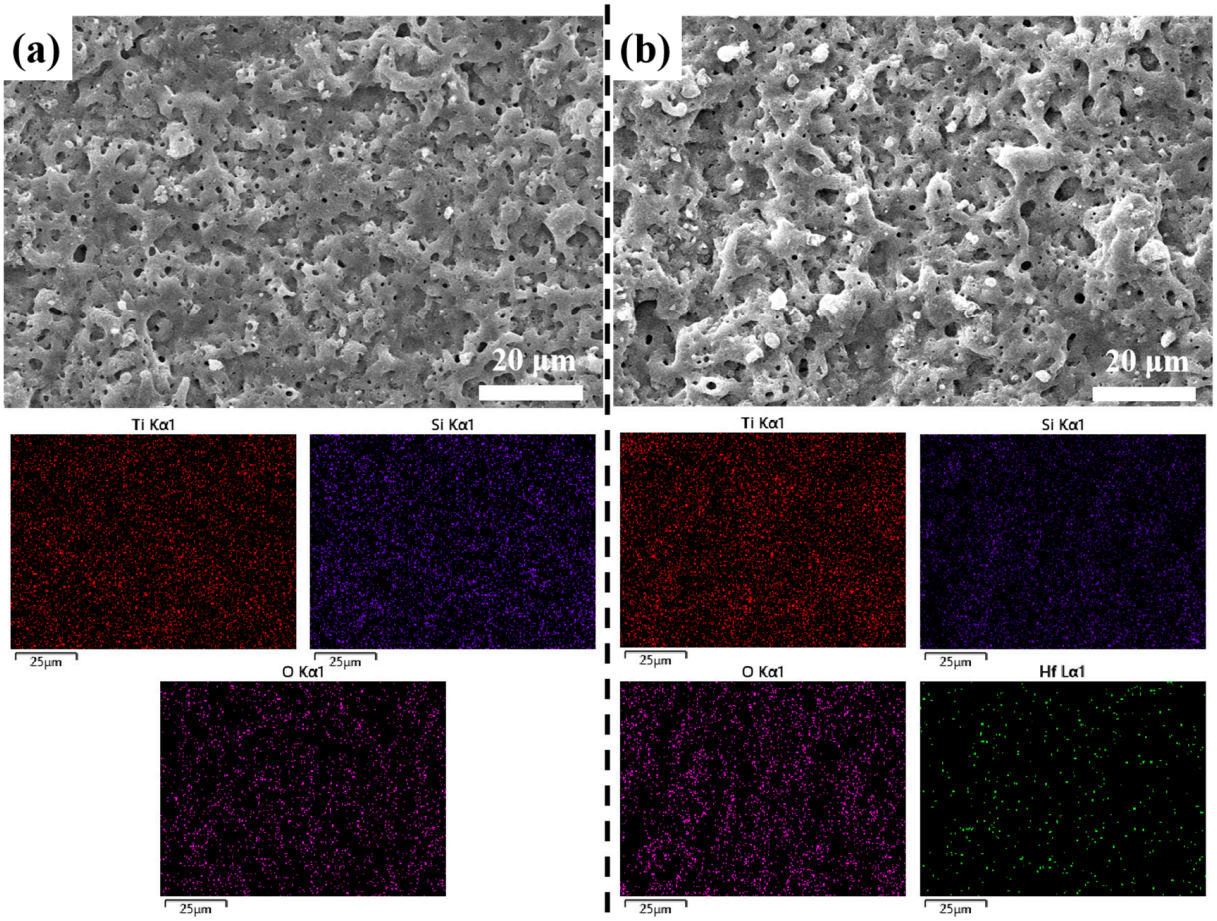

Figure 2. Surface morphology and elements distribution of the (**a**) PEO and (**b**) PEO + HfO_2 coatings.

The EDS mapping results indicated that the Hf element was successfully introduced into the coating (Figure 2b), and the other major components of the PEO coating fabricated on Ti6Al4V were O, Si, and Ti. Table 1 lists the content of each element component of the PEO coatings, and the Hf content of the PEO + HfO_2 coating reached 10 wt.%, which verified that the changes in the microstructure and element content on the surface of the PEO coating were caused by the addition of the HfO_2 particles.

Table 1. The contents of O, Si, Ti, and Hf of the PEO and PEO + HfO_2 coatings.

Element (wt/%)	O	Si	Ti	Hf
PEO	49.4	16.7	33.9	——
PEO + HfO_2	41.6	28.6	19.6	10.2

Figure 3 reveals the cross-sectional morphologies and the element distribution curves from the coating surface to the interior. We found that the coatings and substrates were well bonded, and no explicit boundary existed between the dense and loose sublayers inside the two coatings. The HfO_2-doped coating was denser and thicker (~16 μm) than the nondoped

coating (~8 μm). In general, the oxidation voltage directly affected the deposition rate of the PEO coating: the higher the working voltage during the oxidation process, the faster the deposition rate of the coating, and the greater the thickness of the obtained coating. As shown in Figure 1, the high voltage (~476 V) during the PEO process with the HfO_2 addition provided the necessary energy for the deposition and sintering of the materials. Therefore, the PEO + HfO_2 coating was thicker than the PEO coating prepared under the same conditions.

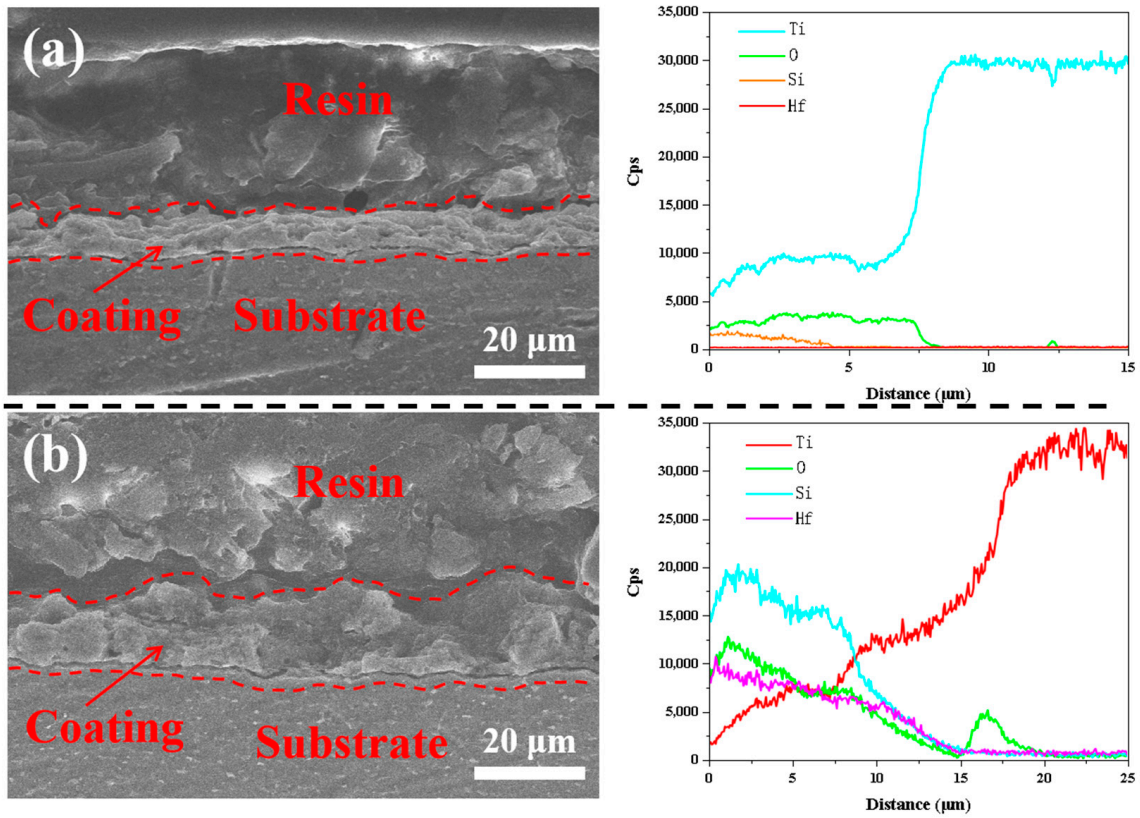

Figure 3. Cross-sectional morphology and elements distribution of the (**a**) PEO and (**b**) PEO + HfO_2 coating.

Regarding the elements' distribution throughout the coating thickness, Ti gradually increased from outside to inside, whereas O, Si, and Hf gradually decreased (Figure 3). By comparison with the nondoped coating, the HfO_2-doped coating (Figure 3b) not only had an obvious Hf diffraction peak (which indicated the successful introduction of Hf into the coating), but it also had a stronger Si diffraction peak. This could be attributed to the more violent plasma electrochemical reaction at a high temperature and pressure.

3.3. Phase Compositions of Coatings

The phase compositions of the PEO coatings are presented in Figure 4. Ti, SiO_2, anatase, rutile, and brookite were the main components. The characteristic peak of Ti appeared in the spectrum because the X-ray could penetrate the coating with micropores to detect the Ti6Al4V substrate. During the PEO process, the inward immigrant O^{2-} could move through the thinner oxidation coating and react with the outward immigrant Ti^{4+} from the substrate to produce the titania ceramics (anatase, rutile, and brookite). The characteristic peak intensity of SiO_2 increased with the addition of HfO_2 particles, which was consistent with the EDS results in Table 1 and Figure 3. This could be explained by the following phenomena: i. the addition of HfO_2 increased the oxidation voltage; ii. more SiO_3^{2-} was electrophoresed to the anode due to the high electric field strength; and iii. the SiO_3^{2-} was sintered by intense plasma discharge and was deposited on the surface of

the anode in the form of SiO_2. Therefore, the amount of SiO_2 precipitation into the oxide layer increased.

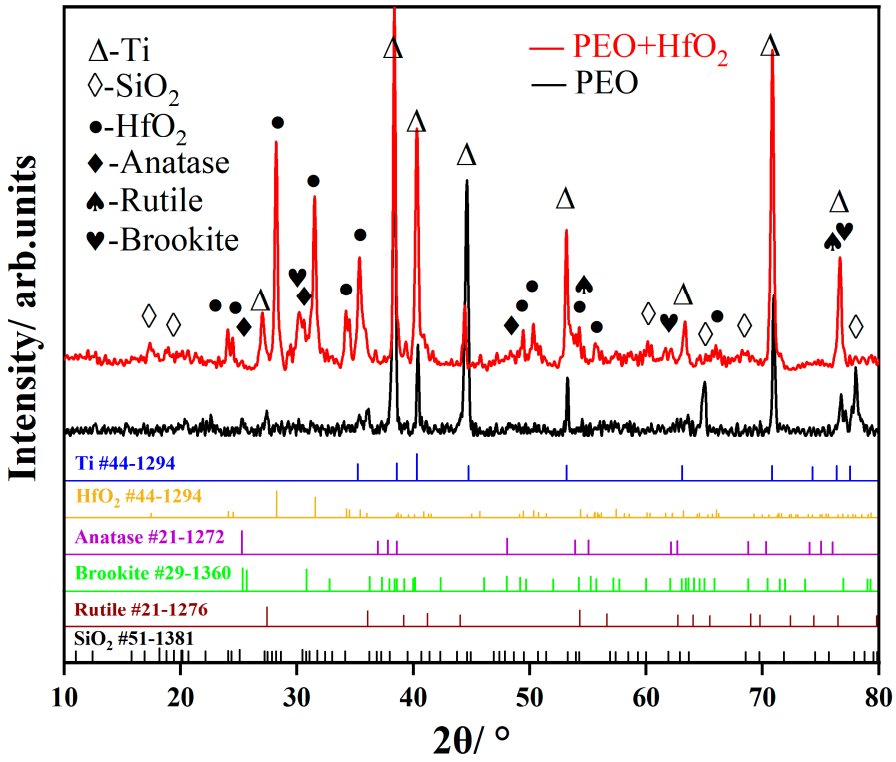

Figure 4. XRD spectra of the PEO and PEO + HfO_2 coatings.

In addition, we found that the Hf introduced into the coating via HfO_2 particles still existed in the form of HfO_2 (Figure 4); specifically, no new phase containing Hf was detected. The temperature of the plasma discharge area was sufficient to melt the HfO_2 particles (melting point of 2758 °C), and therefore the HfO_2 should be metallurgically combined in the PEO coating instead of being mechanically mixed in it in the form of particles. Figure 5 shows the XPS spectrum of the PEO + HfO_2 coating; two fundamental peaks in the Hf4f spectra were clearly observed, which were located at a binding energy of 16.9 and 18.3 eV, which corresponded to $Hf4f_{7/2}$ and $Hf4f_{5/2}$, respectively. The analysis results showed that the Hf element mainly existed in the form of HfO_2 during the microarc oxidation process, and no change in the valence state occurred [25]. According to the results of the EDS, XRD, and XPS analysis above, the following reactions may have occurred during the PEO process:

$$Ti - 4e^- \rightarrow Ti^{4+} \quad (1)$$

$$4OH^- - 4e^- \rightarrow O_2 \uparrow + 2H_2O \quad (2)$$

$$2SiO_3^{2-} - 4e^- \rightarrow 2SiO_2 + O_2 \uparrow \quad (3)$$

$$Ti^{4+} + 4OH^- \rightarrow TiO_2 + 2H_2O \quad (4)$$

$$Ti + 2 > [O] \overset{610\,^{\circ}C}{\rightarrow} TiO_2(\text{Anatase}) \overset{730\,^{\circ}C}{\rightarrow} TiO_2(\text{Rutile}) \quad (5)$$

$$HfO_2(\text{particle}) \overset{\text{micro-arc}}{\rightarrow} HfO_2(\text{melt}) \overset{\text{cooling}}{\rightarrow} HfO_2(\text{coating}) \quad (6)$$

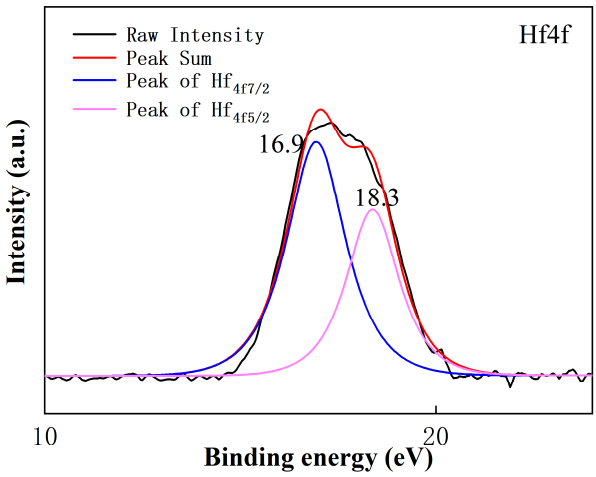

Figure 5. XPS spectrum of the PEO + HfO_2 coating.

3.4. Thicknesses and Microhardnesses of Coatings

The coating microhardness values are provided in Figure 6. With the addition of HfO_2, the hardness of the coating significantly increased, which illustrates that the addition of HfO_2 can increase the deposition rate of the coating during the PEO process (Figure 3). Additionally, the microhardness is generally related to the thickness and grain size [26]. The hardness of the PEO + HfO_2 coating reached ~530 Hv, which contrasts with the ~480 Hv of the PEO coating. The addition of HfO_2 not only refined the grain but also distorted the crystal lattice, which increased the resistance to the dislocation motion and made slip difficult to conduct; thus, the microhardness of the coating was increased.

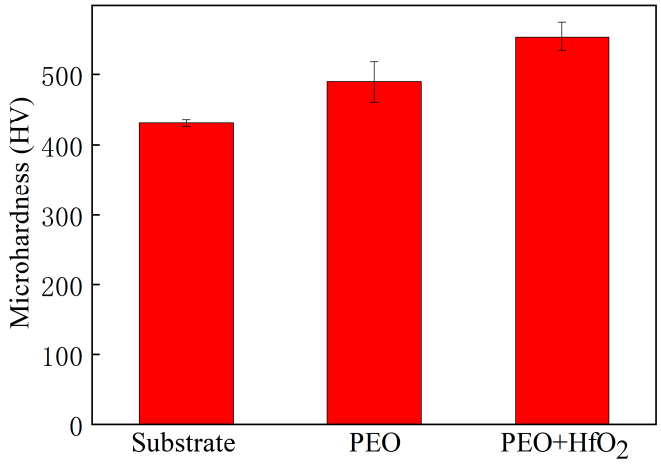

Figure 6. The microhardness of the substrate and the two coated samples.

3.5. Corrosion Resistances of the Coatings

Figure 7 shows the polarization curve of the substrate and the two coated samples. The corrosion current density (I_{corr}) and rate (V_{corr}) were obtained via Tafel fitting according to the Stern-Geary equation (Equation (7), where β_a is the anodic Tafel slope and β_c is the cathodic slope), and Faraday's Law (Equation (8), where N is the equivalent weight and ρ is the density), respectively [7,27]. The results of the Tafel-fitted polarization curves are listed in Table 2. In general, the low E_{corr} and/or high I_{corr} led to a bad corrosion resistance [27,28]. Compared with the coated samples, the substrate's E_{corr} value was the lowest and I_{corr} value was the highest, which implied that the PEO technology can increase the corrosion resistance. Compared with the PEO-coated sample, the E_{corr} value increased from −0.147 to 0.194 V, and the I_{corr} value of the sample treated with the doped HfO_2 decreased from

1.210×10^{-6} to 2.420×10^{-7} A/cm^2. Moreover, the corrosion rate of the PEO-coated sample was two orders higher than that of the sample with HfO_2, which implied that the addition of HfO_2 into the electrolytes was considerably beneficial at preventing the Ti6Al4V alloy from permeating Cl^- ions, which mainly comprise the corrosive medium in the following solution:

$$I_{corr} = \frac{\beta_a \times \beta_c}{\beta_a + \beta_c} \times \frac{1}{R_p} \tag{7}$$

$$V_{corr}\left(\text{mil}\cdot\text{year}^{-1}\right) = \frac{I_{corr}\left(\text{A}\cdot\text{cm}^{-2}\right) \times N(\text{g}) \times \frac{393.7\left(\text{mil}\cdot\text{cm}^{-2}\right)}{\rho\left(\text{g}\cdot\text{cm}^{-3}\right)} \times 365 \times 24 \times 3600\left(\text{m}\cdot\text{year}^{-1}\right)}{96500\left(\text{C}\cdot\text{mol}^{-1}\right)} \tag{8}$$

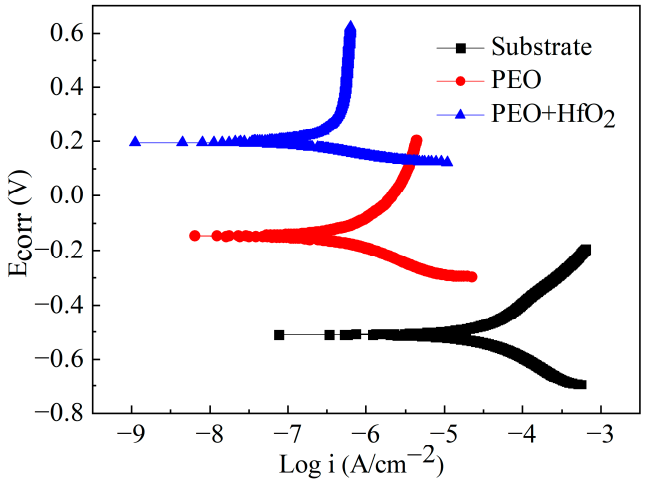

Figure 7. Polarization curves of the substrate and the two coated samples.

Table 2. Results of polarization curve analysis of different samples.

Sample	E_{coor} (V)	I_{coor} (A/cm^2)	Corrosion Rate (mpy)
Substrate	−0.510	4.40×10^{-5}	20.10
PEO	−0.147	1.210×10^{-6}	1.756×10^{-1}
PEO + HfO_2	0.194	2.420×10^{-7}	1.148×10^{-3}

EIS is widely used to evaluate the corrosion mechanism of coatings [28]. Figure 8 shows the EIS Bode plots of the substrate and the two coated samples. In these equivalent circuits, R_S, R_1, and R_2 represent the solution, external layer, and internal layer resistance, respectively. C_1 is the constant phase element of the external layer, and C_2 refers to the constant phase element of the internal layer. The electrochemical parameters of the PEO coatings obtained by using EIS are shown in Table 3. From Table 2, the values of R_1 and R_2 of the sample with HfO_2 were higher, which indicated that adding HfO_2 can remarkably increase the corrosion resistance of the coating, and this was consistent with the results of the Tafel-fitted polarization curves. This result can be attributed to the formation of a relatively thick and less porous coating on the surface of the Ti6Al4V alloy substrate due to the addition of HfO_2 starch into the electrolyte during PEO (Figure 2). Moreover, the presence of more SiO_2 can further enhance the corrosion resistance because this compound has a higher chemical stability in chloride environments.

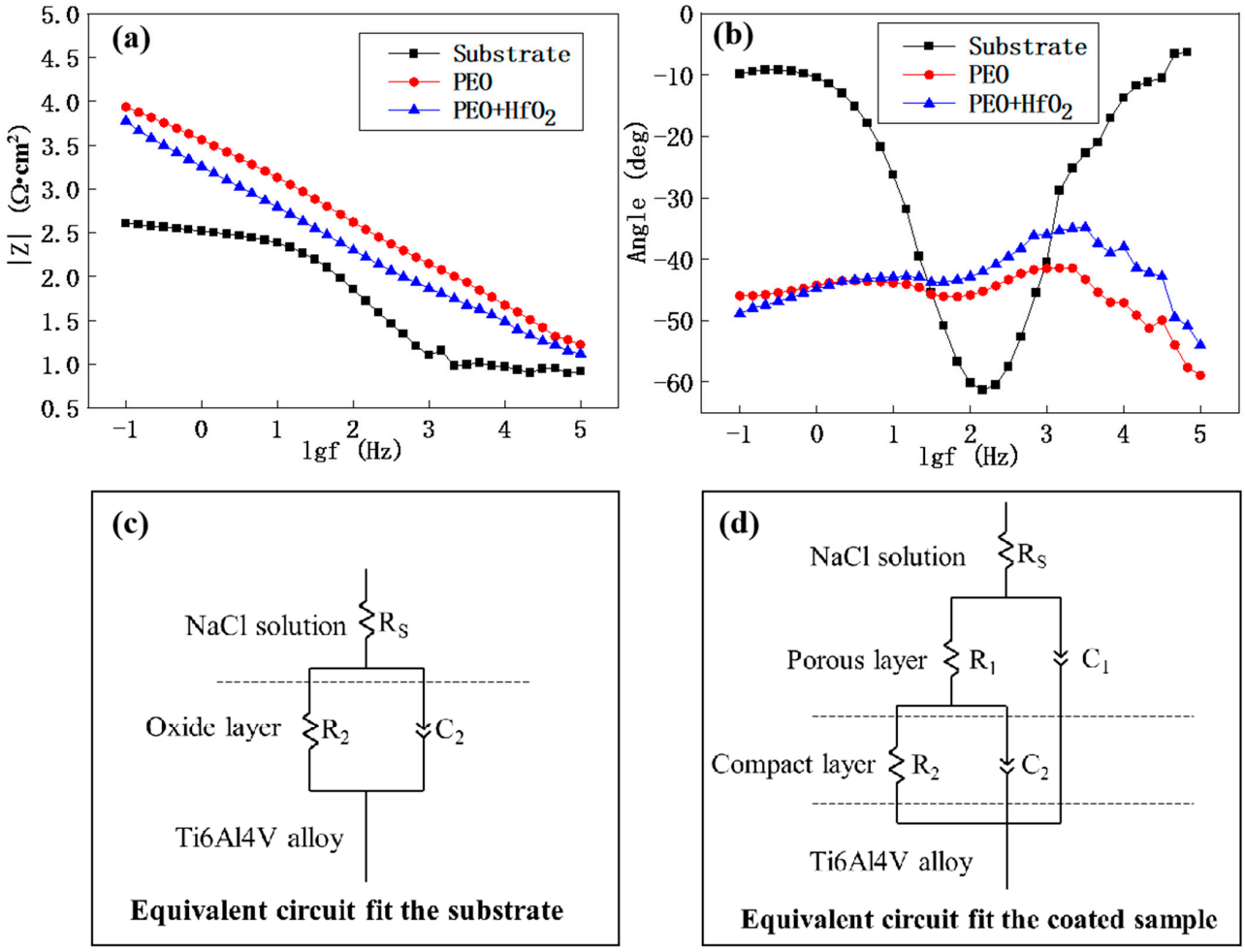

Figure 8. EIS Bode plots and equivalent circuits of the substrate and the two coated samples: (**a**) impedance modulus; (**b**) phase angle; (**c**,**d**) equivalent circuits.

Table 3. Electrochemical parameters of the substrate and the two coated samples.

Sample	R_S ($\Omega \cdot cm^2$)	C_1 ($\Omega^{-1} \cdot cm^{-2}$ S^n)	n_1	R_1 ($\Omega \cdot cm^2$)	C_2 ($\Omega^{-1} \cdot cm^{-2}$ S^n)	n_2	R_2 ($\Omega \cdot cm^2$)
Substrate	9.63	–	–	–	2.146×10^{-5}	0.8276	313.5
PEO	20.5	4.134×10^{-6}	1	302.2	9.454×10^{-6}	0.4739	6468
PEO + HfO_2	41.69	4.145×10^{-6}	0.4498	442	6.13×10^{-5}	0.7793	13,730

In general, the HfO_2-doped PEO coating showed potential applications for the surface protection of the Ti6Al4V alloy. Researchers should focus on optimizing the PEO process, such as by adding different amounts of HfO_2 particles and electrical parameters.

4. Conclusions

A PEO coating was prepared on a Ti6Al4V alloy via plasma electrolytic oxidation with and without HfO_2 in the electrolyte, and the following conclusions may be drawn:

1. With the addition of HfO_2, the breakdown voltage increased from 355 to 367 V, and the plateau voltage increased from 462 to 476 V. The higher oxidation voltage led to more severe discharge and accelerated the coating formation.
2. The HfO_2 could be introduced into the PEO coating through remelting caused by the plasma discharge.

3. The HfO_2-doped PEO coating had fewer discharge micropores with larger sizes. The HfO_2 refined the grain and increased the microhardness of the coating because of the TiO_2 and SiO_2.
4. The HfO_2 implanted into the PEO coating formed on the Ti6Al4V alloy could effectively increase its corrosion resistance.

Author Contributions: Conceptualization, M.S. and H.H.; methodology, M.S. and H.H.; software, M.J.; validation, M.S. and H.H.; formal analysis, M.S.; investigation, B.Y. and Y.L.; resources, M.S. and Y.L.; data curation, M.J.; writing—original draft preparation, M.S. and H.H.; writing—review and editing, H.H.; visualization, M.S.; supervision, P.W. and B.Y.; project administration, M.S.; funding acquisition, M.S. All authors have read and agreed to the published version of the manuscript.

Funding: This work was supported by the Research Foundation for Talented Scholars of Xihua University (No. Z211043 and No. Z212051). And The APC was funded by [No. Z212051].

Data Availability Statement: Not applicable.

Conflicts of Interest: The authors declare no conflict of interest.

References

1. Boyer, R.R. An overview on the use of titanium in the aerospace industry. *Mater. Sci. Eng. A* **1996**, *213*, 103–114. [CrossRef]
2. Diamanti, M.; Sebastiani, M.; Mangione, V.; Del Curto, B.; Pedeferri, M.; Bemporad, E.; Cigada, A.; Carassiti, F. Multi-step anodizing on Ti6Al4V components to improve tribomechanical performances. *Surf. Coatings Technol.* **2013**, *227*, 19–27. [CrossRef]
3. Williams, J.C.; Starke, E.A., Jr. Progress in structural materials for aerospace systems. *Acta Mater.* **2003**, *51*, 5775. [CrossRef]
4. Chen, L.; Jin, X.; Qu, Y.; Wei, K.; Zhang, Y.; Liao, B.; Xue, W. High temperature tribological behavior of microarc oxidation film on Ti-39Nb-6Zr alloy. *Surf. Coatings Technol.* **2018**, *347*, 29–37. [CrossRef]
5. Critchlow, G.; Brewis, D. Review of surface pretreatments for titanium alloys. *Int. J. Adhes. Adhes.* **1995**, *15*, 161–172. [CrossRef]
6. Wang, P.; Wu, T.; Hao, P.; Guo, X.Y. Effect of $NaAlO_2$ concentrations on the properties of micro-arc oxidation coatings on pure titanium. *Mater. Lett.* **2016**, *170*, 171–174.
7. Liu, S.; Chen, J.; Zhang, D.; Wang, Y.; He, Z.; Guo, P. Properties of Micro-Arc Oxidation Coatings on 5052 Al Alloy Sealed by SiO_2 Nanoparticles. *Coatings* **2022**, *12*, 373. [CrossRef]
8. Rodriguez, L.; Paris, J.; Denape, J.; Delbé, K. Micro-arcs oxidation layer formation on aluminium and coatings tribological properties—A Review. *Coatings* **2023**, *13*, 373. [CrossRef]
9. Wang, P.; Gong, Z.Y.; Li, H.L.; Yang, Q.G.; Cao, W.J.; Hu, J.; Pu, J.; Guo, X.Y.; Xiang, D. Effect of $CoSO_4$ on the characteristics of micro-arc oxidation coatings. *Surf. Eng.* **2020**, *36*, 216–224. [CrossRef]
10. Bai, Y.; Park, I.S.; Lee, S.J.; Bae, T.S.; Duncan, W.; Swain, M.; Lee, M.H. One-step approach for hydroxyapatite-incorporated TiO_2 coating on titanium via a combined technique of micro-arc oxidation and electrophoretic deposition. *Appl. Surf. Sci.* **2011**, *257*, 7010–7018. [CrossRef]
11. Li, H.; Sun, Y.; Zhang, J. Effect of ZrO_2 particle on the performance of micro-arc oxidation coatings on Ti6Al4V. *Appl. Surf. Sci.* **2015**, *342*, 183–190. [CrossRef]
12. Guo, Q.; Xu, D.; Yang, W.; Guo, Y.; Yang, Z.; Li, J.; Gao, P. Synthesis, corrosion, and wear resistance of a black microarc oxidation coating on pure titanium. *Surf. Coatings Technol.* **2020**, *386*, 125454. [CrossRef]
13. Yang, W.; Wu, S.; Xu, D.; Gao, W.; Yao, Y.; Guo, Q.; Chen, J. Preparation and performance of alumina ceramic coating doped with aluminum nitride by micro arc oxidation. *Ceram. Int.* **2020**, *46*, 17112–17116. [CrossRef]
14. Chen, Q.; Jiang, Z.; Tang, S.; Dong, W.; Tong, Q.; Li, W. Influence of graphene particles on the micro-arc oxidation behaviors of 6063 aluminum alloy and the coating properties. *Appl. Surf. Sci.* **2017**, *423*, 939–950. [CrossRef]
15. Zheng, Z.; Zhao, M.-C.; Tan, L.; Zhao, Y.-C.; Xie, B.; Yin, D.; Yang, K.; Atrens, A. Corrosion behavior of a self-sealing coating containing CeO2 particles on pure Mg produced by micro-arc oxidation. *Surf. Coatings Technol.* **2020**, *386*, 125456. [CrossRef]
16. Ma, X.; Jin, S.; Wu, R.; Zhang, S.; Hou, L.; Krit, B.; Betsofen, S.; Liu, B. Influence of combined B4C/C particles on the properties of microarc oxidation coatings on Mg-Li alloy. *Surf. Coatings Technol.* **2022**, *438*, 128399. [CrossRef]
17. Liu, J.W.; Wang, P.; Tang, Y.T.; Xiong, D.; Sun, X.Y.; Hu, J.; Gong, Z.Y.; Yang, B.; Gong, Y.B.; Xiang, D. Effect of Bi_2S_3 on Characteristics of Micro-arc Oxidation Coating formed on TC_4 Alloy. *Int. J. Electrochem. Sci.* **2021**, *16*, 150919. [CrossRef]
18. Mueller, M.; Hilpert, K.; Singheiser, L. High temperature corrosion of $MoSi_2$–HfO_2 composites in coal slag. *J. Phys. Chem. Solids* **2005**, *66*, 509–512. [CrossRef]
19. Badawy, W.A.; Al-Kharafi, F.M. The electrochemical behaviour of naturally passivated hafnium in aqueous solutions of different pH. *J. Mater. Sci.* **1999**, *34*, 2483–2491. [CrossRef]
20. Daubert, J.S.; Hill, G.T.; Gotsch, H.N.; Gremaud, A.P.; Ovental, J.S.; Williams, P.S.; Oldham, C.J.; Parsons, G.N. Corrosion Protection of Copper Using Al_2O_3, TiO_2, ZnO, HfO_2, and ZrO_2 Atomic Layer Deposition. *ACS Appl. Mater. Interfaces* **2017**, *9*, 4192–4201. [CrossRef]

21. Esplandiu, M.J.; Patrito, E.M.; Macagno, V.A. Characterization of hafnium anodic oxide films: An AC impedance investigation. *Electrochim. Acta* **1995**, *40*, 809–815. [CrossRef]
22. Xiong, D.; Wang, P.; Shen, X.W.; Liu, J.W.; Yang, B.; Gong, Y.B.; Gong, Z.Y.; Hu, J.; Xiang, D. Addition of $LuCl_3$ for Improving Micro-structure and Corrosion Resistance of Micro-arc Oxidation Coating Formed on 6061. *Int. J. Electrochem. Sci.* **2021**, *16*, 210460. [CrossRef]
23. Huang, H.; Qiu, J.; Sun, M.; Liu, W.; Wei, X. Morphological evolution and burning behavior of oxide coating fabricated on aluminum immersed in etidronic acid at high current density. *Surf. Coatings Technol.* **2019**, *374*, 83–94. [CrossRef]
24. Huang, H.; Wei, X.; Yang, J.; Wang, J. Influence of surface micro grooving pretreatment on MAO process of aluminum alloy. *Appl. Surf. Sci.* **2016**, *389*, 1175–1181. [CrossRef]
25. Li, M.; Jin, Z.-X.; Zhang, W.; Bai, Y.-H.; Cao, Y.-Q.; Li, W.-M.; Wu, D.; Li, A.-D. Comparison of chemical stability and corrosion resistance of group IV metal oxide films formed by thermal and plasma-enhanced atomic layer deposition. *Sci. Rep.* **2019**, *9*, 10438. [CrossRef]
26. Murr, L.; Inal, O. Crystal defects in coatings and their influence on coating properties. *Thin Solid Films* **1979**, *64*, 77–90. [CrossRef]
27. Mareci, D.; Chelariu, R.; Iacoban, S.; Munteanu, C.; Bolat, G.; Sutiman, D. The Estimation of Localized Corrosion Behavior of Ni-Based Dental Alloys Using Electrochemical Techniques. *J. Mater. Eng. Perform.* **2011**, *21*, 1431–1439. [CrossRef]
28. Mareci, D.; Bolat, G.; Istrate, B.; Munteanu, C.; Cailean, A. Effect of thermal oxidation on electrochemical corrosion behaviour of ZrTi alloys for dental applications. *Mater. Corros.* **2015**, *66*, 1529–1535. [CrossRef]